Melillo, A.; Cabrero-Antonino, M.; Navalón Oltra, S.; Alvaro Rodríguez, MM.; Ferrer Ribera, RB.; García Gómez, H. (2020). Enhancing visible-light photocatalytic activity for overall water splitting in UiO-66 by controlling metal node composition. Applied Catalysis B Environmental. 278:1-11. https://doi.org/10.1016/j.apcatb.2020.119345

Enhancing Visible-Light Photocatalytic Activity for Overall Water Splitting in UiO-66 by Controlling Metal Node Composition.

Arianna Melillo,[†] María Cabrero-Antonino,[†] Sergio Navalón,[,†] Mercedes Álvaro,[†] Belén Ferrer,[*,†] and Hermenegildo García[*,†,‡]*

[†]Departamento de Química, Universitat Politècnica de València, Camino de Vera s/n, Valencia 46022, Spain

[‡]Instituto Universitario de Tecnología Química, CSIC-UPV, Universitat Politècnica de València, Av. de los Naranjos, Valencia 46022, Spain

E-mail: hgarcia@quim.upv.es

Keywords: overall water splitting, photocatalysis, visible light photoresponse, UiO-66, trimetallic MOF

Abstract: The photocatalytic activity of a series of five UiO-66 (M: Zr, Zr/Ti, Zr/Ce, Zr/Ce/Ti, Ce) materials for overall water splitting with generation of hydrogen and oxygen has been herein measured. The most efficient photocatalyst for the overall water splitting is the trimetallic MOF UiO-66(Zr/Ce/Ti) which achieves 230 μmol·g^{-1} of H_2 and 110 μmol·g^{-1} of O_2, upon UV light irradiation, and 210 μmol·g^{-1} of H_2 and 70 μmol·g^{-1} of O_2, upon visible light irradiation. This indicates that its photocatalytic activity derives mostly from the visible region of the spectrum (λ > 450 nm). The photocatalytic activity of trimetallic UiO-66(Zr/Ce/Ti) was maintained upon reuse. Kinetics of the charge separated state monitored by transient absorption spectroscopy shows similar deactivation profiles for the five UiO-66 samples, suggesting that it is the charge separation efficiency the main factor responsible for the differences in the photocatalytic activity. The use of methanol as sacrificial agent during the photocatalytic experiments indicated that the high photocatalytic efficiency for overall water splitting in UiO-66(Zr/Ce/Ti) derives from the favorable kinetics of oxygen evolution.

These results show the potential of multimetallic metal-organic frameworks as solar photocatalysts by tuning light absorption towards the visible region.

1. Introduction

Metal-organic frameworks (MOFs)[1-7] in where metal ions or clusters of metal ions are interacting through coordinative bonds with organic linkers in a highly porous, crystalline, solid structure are promising photocatalysts for the production of solar fuels, including hydrogen generation.[8-21] It has been shown that the strong interaction and the rigid environment with a fixed geometry and distance between the metallic node and the organic linkers favor the photoinduced electron transfer from the organic liker to the positively charged metallic nodes, resulting in an efficient charge separation.[8, 22-26] The large diversity of transition metals together with the large number of linkers offer a considerable flexibility in the selection of adequate chromophores to enhance the photocatalytic activity.[8, 14, 18, 24, 27-30] Among the main challenges to overcome, one of them is to increase the visible light photoresponse of MOFs, this property being of particular interest for photocatalytic applications under solar light irradiation.[8, 13, 15, 18, 31-40]

One of the strategies that has been well established in the area is the use of amino substituted organic linkers or the use of mixed ligand (amino functionalized and parent linker) MOFs as visible light photo responsive MOFs.[8]

Another alternative and complementary approach to enhance the photo response is the use of mixed metals MOFs, in where more than one transition metal is present in the metallic node.[25, 41-45] Electron relay from one metal to another can narrow the effective band gap by introducing intra band gap states that can also facilitate photocatalytic activity by increasing the charge separation efficiency and the lifetime of the charge separation state.[25, 44, 46, 47]

One case in where the mixed metal approach has shown its benefits is the case of UiO-66(Zr).[44, 48-52] Theoretical calculations have suggested that the main of bottleneck of its photocatalytic

activity derives from the fact that both the highest unoccupied (LUCO) and the highest occupied crystal orbital (HOCO) in UiO-66 correspond to frontier orbitals mostly located at the organic linker, resulting in a poor efficiency for the linker to metal node charge transfer.[22] Recently, introduction of Ti^{4+} on the node of UiO-66(Zr) has shown that the photocatalytic activity for CO_2 reduction in the presence of sacrificial electron donors of the mixed metal UiO-66 (Zr/Ti) improves in comparison to single metal analogs.[44, 50, 53]

In a series of papers focused on the calculation of the band gap energies and HOCO/LUCO redox potential in UiO structures, Truhlar and coworkers have proposed that Ce^{4+} based UiO-66 should be an efficient photocatalyst due to the low-laying empty 4f orbitals of Ce^{4+} that would correspond to the HOCO of this UiO-66(Ce) material.[42] In addition, metal doping in Ce^{4+}-based MOFs should promote visible light photoresponse in UiO-66 structure by narrowing the band gap.[43] These theoretical calculations also indicate that the LUCO and HOCO energies of the resulting metal doped Ce^{4+}-UiO-66(Zr) should still have enough energy to promote water oxidation and hydrogen generation, respectively,[42, 43] but these predictions still require experimental evidence.

In connection with the use of MOFs as solar light photocatalysts for overall water splitting,[54-58] our group has shown that besides hydrogen generation in the presence of sacrificial electron donors,[56] MOFs can also generate oxygen photocatalytically from H_2O in the absence of electron acceptors, a more challenging process than simple hydrogen generation in the presence of electron donors .[56] It is clear that real application of MOFs for the production of solar fuels requires the simultaneous stoichiometric generation of hydrogen and oxygen from water.

Continuing with this line of research and led by the theoretical calculations showing that modification of node composition can result in alteration of the bandgap,[42, 43] the present manuscript reports the solar and visible light photocatalytic activity for overall water splitting of mixed-metal UiO-66(Zr/Ce/Ti) solids. Only a few reports have shown that MOFs are able to promote the photocatalytic overall water splitting, but the production rates with simulated sunlight up to now are low, about 100 $\mu mol \times g_{catalyst}^{-1}$.[56] Also the photoresponse was almost exclusively

due to the UV light. In contrast to these precedents, the present study reports a high overall water splitting activity mostly in the visible region due to the node composition with the three transition metals with respect to the mono and bimetallic analogs. The present study shows the opportunity that MOFs offer to tune their photocatalytic activity in the visible region and increase the photocatalytic efficiency by developing sites that favor four electrons/four protons required in water oxidation. Fluorescence and time-resolved absorption spectroscopy provide evidence showing that the charge separation is favorable in the case of the trimetallic UiO-66(Zr/Ce/Ti). In this way the photocatalytic activity for overall water splitting for the trimetallic UiO-66(Zr/Ce/Ti) for the visible light increases about one order of magnitude with respect to the parent UiO-66(Zr). Overall, the experimental data are in general agreement with the theoretical prediction and illustrate the versatility and potential of MOFs as photocatalysts.

2. Material preparation and characterization

The materials under study, their preparation and the characterization data will be described in the first place, before commenting on their photocatalytic activity in overall water splitting.

Five different UiO-66 containing either Zr or Ce and mixed bimetallic Zr/Ce, Zr/Ti and trimetallic Zr/Ce/Ti were prepared in the present study. Four of them, mono and bimetallic UiO-66(Zr), UiO-66(Ce), UiO-66(Zr/Ce) and UiO-66(Zr/Ti) materials have been already described in the literature and were prepared following the corresponding reported procedures, [44, 51, 59, 60] while UiO-66(Zr/Ce/Ti) was synthesized for the first time in this work.

UiO-66: The synthesis of Zr-BDC MOF was carried out dissolving the metallic salt $ZrCl_4$ (0.053 g, 0.227 mmol) and the organic linker 1,4-benzenedicarboxylic acid (H_2BDC) (0.034g, 0.227 mmol) in *N*,*N*`-dimethylformamide (DMF) (24.9 g, 340 mmol) at room temperature. The mixture was transferred in a Teflon-lined autoclave, sealed and placed in a pre-heated oven at 120℃ for 24 hours. After cooling to room temperature, the resulting white solid was filtered and washed several times with DMF and dried at room temperature.

UiO-66(Zr/Ti): UiO-66 (Zr/Ti) was synthetized following a post-syntetic method using $TiCl_4(THF)_2$ under inert atmosphere. Synthesized UiO-66 (0.45mmol) and $TiCl_4$(0,135mmol) as Ti source were suspended in 2.5 mL DMF and incubated for 4 days at 120 °C. After cation exchange, the corresponding UiO-66 (Zr/Ti) solids were filtered, washed sequentially with DMF and MeOH and dried in vacuum at 40 °C for 24 hours.

UiO-66(Zr/Ce): UiO-66 (Zr/Ce) MOF was synthesized using Pyrex glass reaction tubes. H_2BDC, (127.6 mg) was introduced into the glass reactor with DMF (3.6 mL) and aqueous solutions of cerium(IV) ammonium nitrate (0.533 M; 117 mg, 0.400 mL water), zirconium(IV) dinitrate oxide hydrate (0.533 M, 99.0 mg 0.800mL) and concentrated formic acid (HCOOH, 100 %, 1.03 mL) were added. The suspension of the starting materials was heated under stirring for 15 min at 100 °C. The light-yellow precipitate was centrifuged in the mother solution and then it was decanted off. The solid was centrifuged twice in DMF (2 mL) and then, to remove DMF, the solid was washed and centrifuged with acetone (2 mL) four times. The resulting white solid was dried in air at 70 °C.

UiO-66(Zr/Ce/Ti): UiO-66(Zr/Ce) (0.45mmol) and $TiCl_4(THF)_2$ (0.135mmol) as Ti source were suspended in 2.5 mL DMF and incubated for 4 days at 120 °C. After cation exchange, the resulting UiO-66(Zr/Ce/Ti) solids were filtered, washed sequentially with DMF and MeOH and dried in vacuum at 40 °C for 24 h.

UiO-66(Ce): H_2BDC (35.4 mg, 213 μmol) was introduced into the glass reactor with DMF (1.2 mL) and an aqueous solution of cerium (IV) ammonium nitrate (400 μL, 0.5333 M). The glass reactor was heated under stirring conditions for 15 min at 100 °C. The light-yellow precipitate was centrifuged in the mother suspension; then, the solid was centrifuged twice in DMF (2 mL). To remove DMF from the product, the solid was washed and centrifuged with acetone (2 mL) four times. The resulting yellow solid was dried in air at 70 °C.

Scheme S1 shows the route followed for the preparation of these five UiO-66 samples. Three of them were prepared *de novo* in a single step using terephthalic acid and either $ZrCl_4$, $Ce(NH_4)_2(NO_3)_6$ or a mixture of both as described in the literature.[44, 51, 59, 60] It should be noted that for the case of UiO-66(Zr/Ce), with Zr/Ce atomic ratio of 4, exhaustive characterization by elemental analysis and XPS has provided conclusive evidence supporting the location of the two metals at the nodes of the MOF.[59, 61] The two Ti^{4+} containing samples were prepared by post-synthetic ion exchange in

dimethylformamide (DMF) as previously described,[44, 50, 60] starting either from UiO-66(Zr) or the bimetallic UiO-66(Zr/Ce) and using the $TiCl_4(THF)_2$ complex as Ti source in DMF at 120 ºC.

Table 1 lists the samples under study and summarizes some of the relevant analytical and textural data obtained from ICP-AES, BET surface area and pore volume measurements (representative isotherm curves are shown in **Figures S1-S3**).

Table 1. List of the photocatalysts employed in this work indicating the metal content per formula, specific BET surface area and pore volume values.

MOF	Zr (mol)	Ti (mol)	Ce (mol)	Sum of moles	BET (m^2/g)	Pore Volume (cm^3/g)
UiO-66(Zr)	6.34	/	/	6.34	1258	0.75
UiO-66(Zr/Ti)	4.82	0.84	/	5.66	974	0.78
UiO-66(Zr/Ce)	5.64	/	0.91	6.55	1297	0.69
UiO-66(Zr/Ce/Ti)	4.16	1.18	0.5	6.46	1019	0.65
UiO-66(Ce)	/	/	5.6	5.6	916	0.35

The isomorphic crystal structure of the samples corresponding to the UiO-66 structure was confirmed by powder X-ray diffraction (PXRD). Supporting information presents the PXRD patterns recorded for the five samples (**Figure S4-S5**). Some small, but significant, shifts in the position of the lowest angle diffraction peak from 7.2 º for UiO-66(Ce) to 7.4 º for UiO-66(Zr) and UiO-66(Zr/Ce) till 7.5 º for UiO-66(Zr/Ti) and UiO-66(Zr/Ce/Ti) were observed. As a general trend, the replacement of Zr^{4+} or Ce^{4+} ions by smaller Ti^{4+} ones at the metal node causes some contraction of the unit cell, as confirmed by the crystallographic data shown in Figure S2. Comparison of the diffractograms b and d in Figure S2 shows for both MOFs containing Ti a shift

of the peak at 7.4 º to a value of 7.5 º. This small shift in the position of the shortest angle diffraction peak has been already observed in the literature and attributed to the incorporation of Ti^{4+} having the small ionic radius to the nodes.[44] Similar observations have been previously reported in the literature, and taken as an evidence of the framework incorporation metals.[25, 44, 60, 62, 63] The average crystal size of the photocatalyst UiO-66 (Zr / Ce / Ti) was further analyzed through the use of the Scherer formula and on the basis of a detailed evaluation of the X-ray diffractogram.

$$D = k \cdot \lambda \, / \, \beta cos\theta$$

Where:

D= crystallites size (nm)

K= 0.9 (Sherrer costant)

λ= 0.15406 nm (Wavelength of X-ray sources)

β = FWHM (radiants)

θ = peak position (radiants)

The calculation was supported by the Origin 8 program and provides a value of 9. 71 nm, which is consistent with the value that has been previously estimated through structural analyzes only.

The nature and content of the transition metals present in the material was determined by ICP-AES and the results obtained are listed in **Table 1**. The difference between the theoretical metal content of 6 mols of metal for the ideal formula $Zr_6(\mu_3\text{-}O)_4(\mu_3\text{-}OH)_4(\mu_4\text{-}BDC)_6]n$ (BDC: benzene-1,4-dicarboxylate) and the experimental value (**Table 1**) is generally assumed as due to the presence of defects on the UiO-66 sample.[64] Importantly, the incorporation of Ti atoms on the UiO-66(Zr) and UiO-66(Zr/Ce) solids is accompanied by a decrease of Zr or Zr and Ce content of the materials. XRD and ICP-AES analysis agree with previous reports in the literature describing the partial replacement of Zr^{4+} or Ce^{4+} atoms present in the UiO-66(Zr)[63] or UiO-66(Ce) solids,[62] respectively, by Ti^{4+}atoms.

The density of defects in the series of UiO-66 was estimated by thermogravimetry, determining the residual remaining weight of the material after combustion of the organic linkers, corresponding to metal oxides, that was compared to the theoretical amount according to the expected unit cell formula. **Figure S6** contains the thermogravimetric profile of each of the different UiO-66 MOFs under study.

Surface area and porosity were determined by isothermal nitrogen adsorption at 77 K (**Figures S1-S3).** The data are contained in **Table 1**. It was found that UiO-66(Zr) and UiO-66(Zr/Ce) were the materials with the largest specific surface area above 1200 m^2/g. The smallest BET area corresponds to UiO-66(Ce) that has a value of 916 m^2/g in good agreement with previous reports.[65] The two samples containing Ti^{4+} have an area that is in between these values. While the pore volume of four of the samples was about 0.7 cm^3/g, this value was about 0.4 in the case of UiO-66(Ce), again in accordance with the data previously described in literature.[66] The BET surface area and pore volume data are listed in Table 1. Analysis of these data shows that the surface area values of UiO-66(Zr) and UiO-66(Zr/Ce), both samples prepared by *de novo* synthesis, are comparable. This indicates that the partial exchange of Zr^{4+} by Ce^{4+} in the proportions present in UiO-66(Zr/Ce) does not influence material porosity. This conclusion is in agreement with the coincidence of XRD patterns for UiO-66(Zr) and UiO-66(Zr/Ce). Particularly, the comparison of the diffractograms (a) and (c) in Figures S1 and S2 clearly indicates that the two MOFs are isostructural. In addition, the pore volume of the two materials are similar, going from 0.75 cm^3/g for UiO-66(Zr) to 0.69 cm^3/g for UiO-66(Zr/Ce). The small decrease of the pore volume could be related to somewhat larger metal nodes due to the larger cation radius of Ce^{4+} respect to Zr^{4+}. However, the fact that the Ce^{4+} percentage is less than 20 % does not cause large structural distortions. On the other hand, for UiO-66(Ce), also prepared by *de novo* synthesis using a Ce^{4+} salt, the larger Ce^{4+} cation radius compared to Zr^{4+} is responsible for larger structural distortions reflected in the diffractogram of the samples (Figure S2) also causing a diminution of the BET surface area, 916 m^2/g, and the pore volume of the material, 0.35 cm^3/g, for UiO-66(Ce).

Regarding Ti^{4+}, the partial replacement of Zr^{4+} and/or Ce^{4+} by Ti^{4+} cation is reflected in a substantial decrease in the surface area value of the material, but a constant pore volume size. These variations in the porosity indicate the formation of defects and distortions of the crystal structure.

IR spectroscopy shows some variation in the relative intensity of a specific peak of the terephthalate linker appearing at 1590 cm^{-1} and corresponding to the stretching vibration of the -C(O)O group, that depends on the nature of the transition metal at the node. This peak splits in two bands for UiO-66(Zr/Ti) and shifts to higher wavenumber for UiO-66(Zr/Ti/Ce) and UiO-66(Zr/Ce) This variation in IR spectrum is in agreement with the replacement of Zr^{4+} in the inorganic node of bimetallic and trimetallic MOFs by Ti^{4+} and Ce^{4+} ions. **Figure S7** in the supporting information contains the IR spectra of the five samples under study and the area where the previously mentioned variation of the peak can be observed has been marked.

The morphology of the particles was observed by field-emission scanning electron microscopy (FESEM), scanning transmission electron microscopy (STEM) and transmission electron microscopy (TEM) (**Figures S8-S21** in supporting information). These images show that UiO-66(Zr) is constituted by cubes of about 70 nm size together with smaller particles. Similarly, UiO-66(Zr/Ce) exhibits cuboctahedra particles of about 20 nm together with some larger particles. In the case of UiO-66(Ce), the particles have smaller size and ill-defined geometrical shape. The morphology of the particles changes upon ion exchange with Ti^{4+} in DMF, resulting in smaller particles with non-defined planes. STEM and TEM images show…….. EDX elemental analysis of the particles shows the uniform distribution of the metals in the crystals. In particular, EDX elemental analysis of the trimetallic UiO-66(Zr/Ce/Ti) MOF (**Fig. S17**) coincides with the theoretical elemental analysis. The slightly higher experimental value, compared with the theoretical one, obtained for the Ti content could be explained by the post-synthetic introduction of Ti in the metallic node that leaves some Ti content in the external surface of the solid.

The series of the UiO-66 solids were also characterized by XPS. This technique reveals the presence and oxidation state of the atoms present in the solids. Some general XPS features for all the UiO-66 materials prepared can be drawn (**Figures S22-S26** in supporting information). Thus, C1s XPS shows the presence of aromatic carbons (~284.4 eV), together with carboxylate carbon atoms (~288 eV) of the terephthalate ligands. The O 1s XPS band centered at about 532 eV is mainly due to the oxygens present at the carboxylate groups. The Zr 3 $d_{5/2}$ (182.5 eV) and 3 $d_{3/2}$ (184.5 eV) are characteristic of the Zr^{4+} atoms present in the metal nodes. XPS Ti 2p confirms Ti^{4+} incorporation in the metal nodes as revealed by the XPS Ti $2p_{3/2}$ (~458 eV) and $2p_{1/2}$ (~464 eV). Regarding the characterization of Ce atoms in the UiO-66 solids, previous studies have reported the presence of Ce^{3+} atoms together with Ce^{4+} in the single-metal UiO-66(Ce) material based on XPS.[51] The same mixed Ce^{3+}/Ce^{4+} valence state was also observed for mixed-metal UiO-66(Zr/Ce) solids, where Zr^{4+} substitution at the nodes by $Ce^{4+/3+}$ was previously supported by X-ray absorption near edge structure spectroscopy.[51] In our study, the three XPS Ce 3d bands at 884, 901 and 917 eV can be attributed to Ce^{4+} ions at the metal nodes.[51, 66]

One important issue to be addressed in mixed-metal MOFs is the location of metals in the secondary building units (SBUs).[67] One possibility is that the metals are arranged in different SBUs, while a second possibility is that the metals are randomly distributed sharing the same SBUs. Based on previous studies about mixed-metals, mixed-metal SBUs are more likely to be formed for metal ions of similar ionic radio and affinity to coordinate oxygen atoms. Thus, in principle the mixed-metal SBU would be more favorable when using Zr^{4+} and Ti^{4+} atoms, respect to Zr^{4+} and Ce^{4+}. In fact, previous reports using UiO-66(Zr/Ce) have concluded that the more favorable configuration of this MOF would contain Zr_6 and Ce_6 nodes although mixed-metal SBU of $CeZr_5$ can be present.[68]

In principle, in the case of the UiO-66(Zr/Ce/Ti) material the metal clusters could be constituted by one, two or three different metals. XPS has been reported as an appropriate technique to support the distribution of metals, depending on whether or no changes in the binding energy and symmetry of

the XPS peaks corresponding to the different metal ions are observed.[67] Metals present in different SBUs should exhibit the same XPS peaks as those of single-metal MOFs since the interaction among these metal ions should be negligible because they are separated by the terephthalate units. In contrast, the presence of two or three different metals in the same SBU could be reflected in differences in the XP spectra of the mixed-metal MOF compared to the monometallic MOF. Comparison of XPS Zr 2p peaks for the UiO-66 series (**Figure S27**) show a shift (0.32 eV) in the Zr binding energy in the case of UiO-66(Zr/Ti) and UiO-66(Zr/Ce/Ti) respect to the parent UiO-66(Zr) that is not observed, as already reported, in the case of the UiO-66(Zr/Ce). In contrast, the XPS Ti 2p peak of UiO-66(Zr/Ti) and UiO-66(Zr/Ce/Ti) are coincident in binding energy **(Figure S27)**. These findings agree with the presence of mixed-metal SBUs of Zr and Ti atoms in the UiO-66 solids while Zr and Ce atoms should be located in isolated domains. Furthermore, XPS Ce 3d peak of UiO-66(Ce) and UiO-66(Zr/Ce) are very similar **(Figure S27)**, as reported[61, 68] while in the case of UiO-66(Zr/Ce/Ti) the binding energy for Ce decreases, indicating that Ce is sharing node with Ti as previously reported for the UiO-66(Ce) partially exchanged with Ti^{4+} in the metal node.[62] In summary, XPS analysis of the samples are coincident with the literature in the case of UiO-66(Zr/Ce) where separate Zr_6 and Ce_6 nodes are present, but indicates that Ti shares nodes both with Zr and Ce.

Regarding the photocatalytic activity, one important information that indicates which are the photons absorbed by the material is the UV-Vis absorption spectra. These absorption spectra recorded in the diffuse reflectance mode are presented in **Figure 1**. It can be seen there that the sample absorbing at longer wavelength is the UiO-66(Ce), in agreement with theoretical data that have predicted a narrowing of the LUCO that HOCO band gap for this material in comparison to UiO-66(Zr).

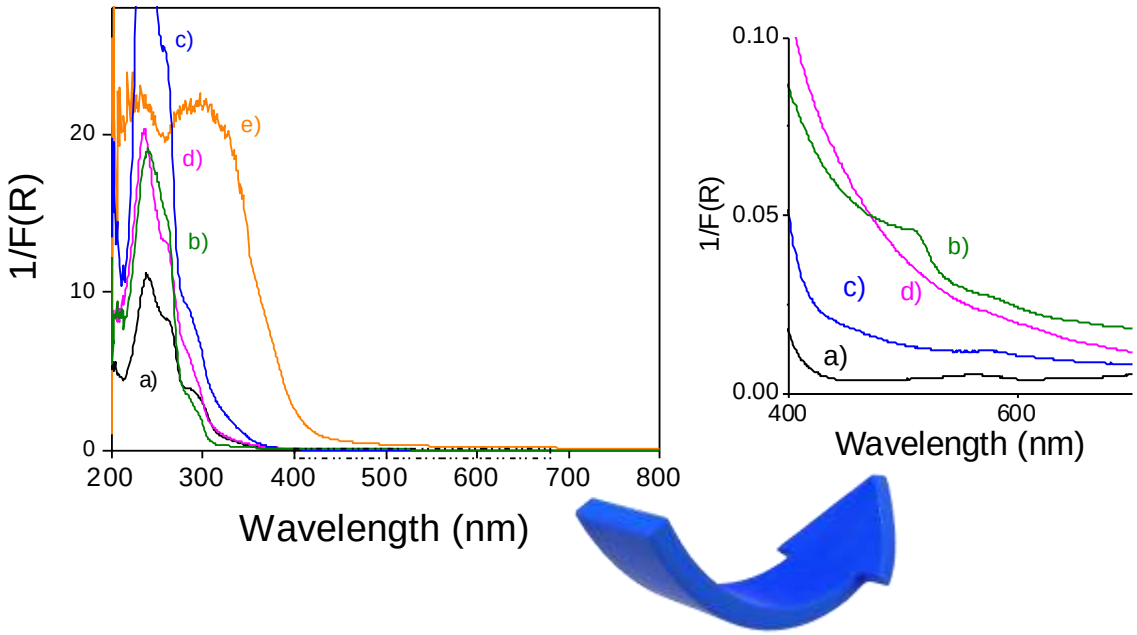

Figure 1. Diffuse reflectance UV-Vis spectra of a) UiO-66(Zr), b) UiO-66 (Zr/Ti), c) UiO-66(Zr/Ce), d) UiO-66(Zr/Ce/Ti), e) UiO-66(Ce). The inset (at right) corresponds to a magnification of the 400-650 nm region for plots a, b, c and d.

In addition, as it can be seen also in **Figure 1**, an expansion of the absorption spectrum onset shows that the introduction of titanium on the node produces a red shift of the onset respect to the parent UiO-66(Zr) and the trimetallic UiO-66(Zr /Ce/Ti) has an absorption tail that expands up to 600 nm into the visible zone. The estimated band gap values from diffuse reflectance UV-Vis spectroscopy (**Figure S28**) for UiO-66(Zr), UiO-66(Zr/Ce), UiO-66(Zr/Ti), UiO-66(Zr/Ce/Ti) and UiO-66(Ce) are 3.31, 3.25, 3.10, 3.05 and 2.60 eV, respectively. In particular, the band gap of UiO-66(Zr/Ce) is close to that of UiO-66(Zr) while UiO-66(Zr/Ti) and UiO-66(Zr/Ce/Ti) exhibit slightly smaller band gap values. According to previous studies[67] and in agreement with our XPS and XRD data it is proposed that the presence of Ti^{4+}in the same SBU as Zr^{4+} and $Ce^{4+/3+}$ is responsible of the band gap narrowing respect to the UiO-66(Zr) solid.[67]

3. Results and discussion

3.1. Photocatalytic activity

The samples under study were screened for their photocatalytic activity for overall water splitting upon irradiation with a xenon lamp (UV-Vis) in the absence (**Figure 2a**) or in the presence (**Figure 2b**) of a cutoff filter (λ> 450 nm). The results obtained under these two conditions after 24 h irradiation is presented in **Figure 2**.

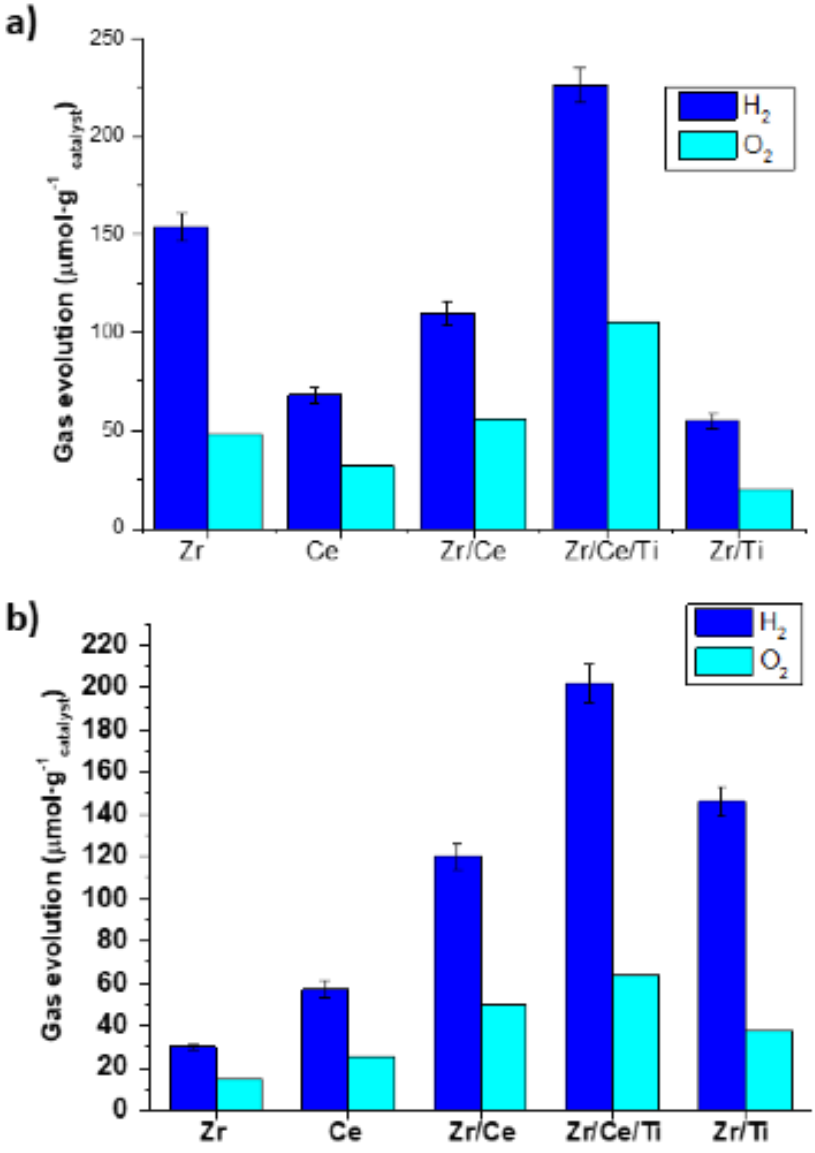

Figure 2. Photocatalytic gas evolution using different UiO-66 as photocatalysts upon irradiation with UV-visible light (a) or exclusively with visible light (b) (λ> 450 nm). Reaction conditions: light source UV-Vis xenon lamp (150 mW cm^{-2}) equipped or not with a filter (λ> 450 nm), photocatalyst 20 mg, H_2O (20 mL) photoreactor volume (51 mL), reaction temperature (35 °C).

As it can be seen in **Figure 2**, in all cases evolution of hydrogen and oxygen was observed. In general, the amount of oxygen was close to the expected stoichiometric amount according to the evolution of hydrogen. Similar lesser O_2 formation has been frequently observed in the literature and attributed to adventitious hole and/or oxygen consumption.[56] This less than expected O_2 production is motivated by the high oxidation potential required in water oxidation and its slow kinetics. The lesser than expected O_2 evolution can be due to the partial consumption of holes causing some oxidation of metal sites of the photocatalyst, or the binding and consumption of some formed O_2 with metal nodes or photoreactor.

Several remarkable facts were observed when comparing the performance of the different samples. Thus, comparison of part a and b in **Figure 2** shows that the photocatalytic activity of UiO-66(Zr) derives mainly from the UV region, decreasing significantly when using exclusively visible light. This is in agreement with the poor photoresponse of UiO-66(Zr) for most of the visible light photons. It is also remarkable that the photocatalytic activity of UiO-66(Ce) remains almost the same when the sample is irradiated in the UV-visible or the visible region, meaning that in the case of UiO-66(Ce) the photoresponse derives mainly from visible light, therefore contrasting with the behavior of UiO-66(Zr). Similar performance of almost constant photocatalytic activity under UV-Vis or visible light irradiation was also observed for the other three samples, namely UiO-66(Zr/Ce), UiO-66(Zr/Ti) and UiO-66(Zr/Ce/Ti). The photocatalytic activity for overall water splitting follows the order UiO-66(Zr/Ce/Ti)>UiO-66(Zr/Ti)>UiO-66(Zr/Ce).

Overall, these photocatalytic data show the remarkable increase in visible light activity achieved by introduction of Ti^{4+} into the parent UiO-66(Zr). As it can be seen in **Figure 2b**, the best performing UiO-66 was the trimetallic UiO-66(Zr/Ce/Ti), showing the benefit on the photocatalytic activity of introducing more than two metals. Overall, the photocatalytic activity of UiO-66(Zr/Ce/Ti) is seven- time higher than that of UiO-66(Zr). To put the obtained values into context, recently our group has reported a hydrogen production from overall water splitting using MIL-125(Ti)-NH_2 and MIL-125(Ti)-NH_2 simultaneously loaded with Pt and RuOx NPs as co-catalysts values of 48 and

218 μmol g^{-1} respectively, after 24 h under similar reaction conditions as there used in the parent study.[56] The values presented in the **Figure 2b** for UiO-66(Zr/Ce/Ti) are similar to those reported by Pt, RuO_3-MIL 125 (Ti)-NH_2, but using exclusively visible light and in the absence of any precious metal. Thus, the results achieved in **Figure 2b** are remarkable and probably among the highest ever reported with visible light.

To understand better the reasons of the higher activity of the trimetallic UiO-66(Zr/Ce/Ti) with respect to the other related congeners, an additional experiment with monochromatic light at 400 nm was performed. This wavelength is at the limit of the visible region and corresponds to the onset of the absorption band for the four-zirconium containing UiO-66 (**Figure 1**) and the absorption intensity at this wavelength follows the same relative order as the photocatalytic activity measured for the full visible wavelength range. It is, therefore, proposed that light absorption is one of the main factor determining the relative photocatalytic activity order in the case of the Zr containing MOFs. However, the fact that UiO-66(Ce) exhibits even higher visible absorption, but it is much less active indicates that the multimetallic composition of the nodes should also play and important role. In addition, the photoresponse of UiO-66(Zr/Ce/Ti) for overall water splitting was measured for three wavelengths namely 300, 400 and 500 nm (**Figure 3**), observing that the highest relative efficiency corresponds to 400 nm.

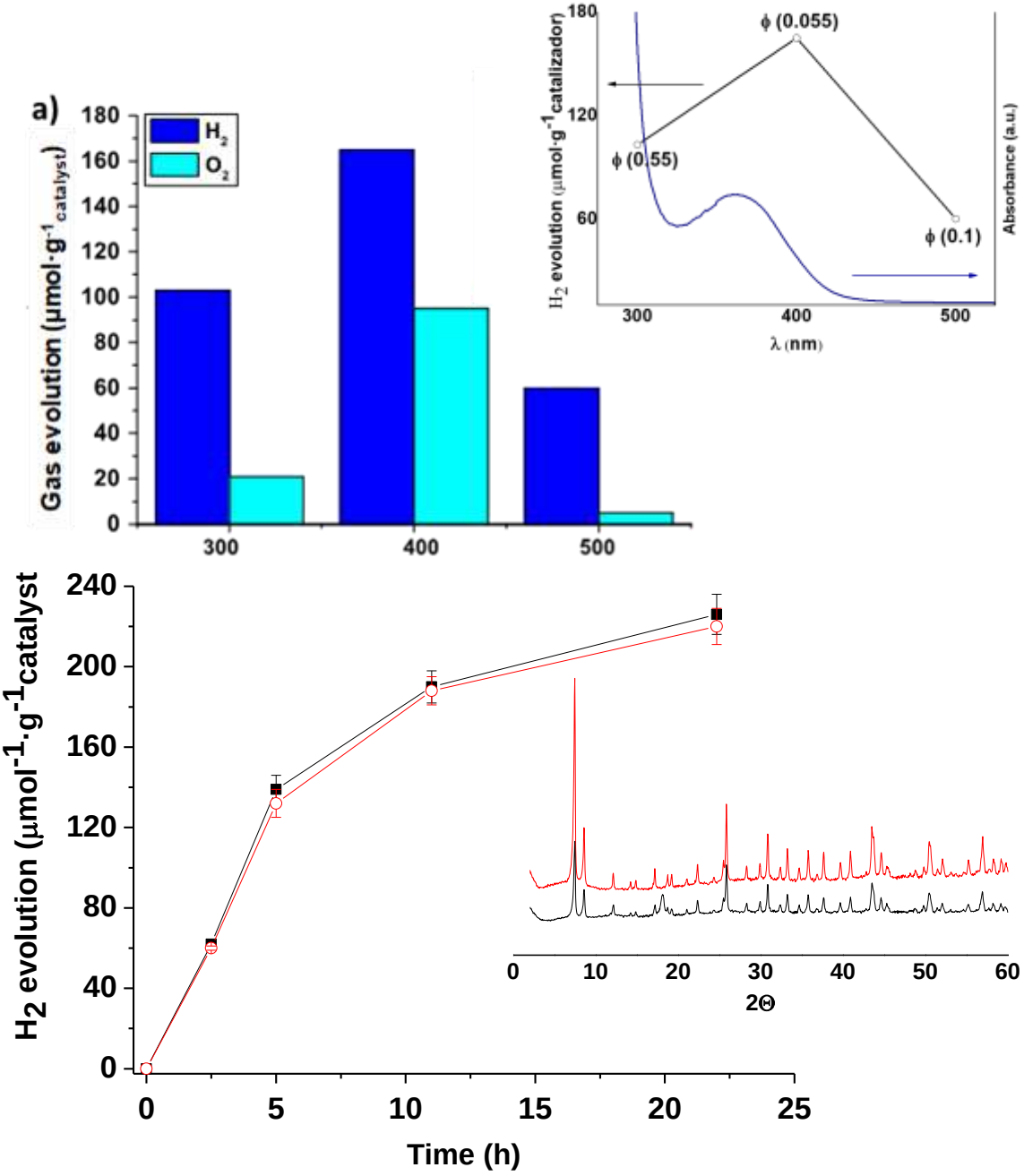

Figure 3. a) Overall water splitting using UiO-66(Zr/Ce/Ti) under monochromatic irradiation (300, 400 or 500 nm). Inset: H_2 production upon monochromatic light irradiation and the corresponding UV-Vis diffuse reflectance spectra of UiO-66(Zr/Ce/Ti). The values of the energetic efficiency for each wavelength, obtained by the equation S1, are given in the graph. Reaction conditions: UiO-66(Zr/Ce/Ti) (10 mg), Milli Q-H_2O (10 mL), temperature (35 °C), and reaction time: 22 h. b) Photocatalytic H_2 evolution in the overall water splitting for two consecutive uses of UiO-66(Zr/Ce/Ti): first use (■); second use (○). The inset shows the XRD of the fresh (black one) and two-times used (red one) UiO-66(Zr/Ce/Ti) sample. Reaction conditions: catalyst (20 mg) light source UV-Vis xenon lamp (150 mW cm-2) with a cut off filter (λ> 450 nm), H_2O (20 mL) photoreactor volume (51 mL), reaction temperature (35 °C).

Regarding stability, the same sample of UiO66 (Zr/Ce/Ti) was submitted to two consecutive uses as photocatalyst under visible light irradiation ($\lambda > 450$ nm), following the temporal profile of hydrogen and oxygen evolution (**Figure 3b**). A minor decrease in the initial reaction rate and final hydrogen production was observed that could be due to the incomplete recovery of the material after the run to be used as a photocatalyst in the subsequent reaction or to the analytical experimental error. In addition, XRD shows no change in the position or intensity of the diffraction peaks of the fresh and two times used samples.

The overall water splitting consists in the simultaneous production of hydrogen by conduction band electrons and the corresponding amount of oxygen by valence band holes. Typically, to increase the efficiency of a photocatalyst it is convenient to add a co-catalyst whose role is to facilitate interfacial electron transfer, and evolution of gases, increasing in this way the efficiency of the photocatalytic process. Typical co-catalysts are noble metals such as platinum, palladium and gold or critical metals such as ruthenium or cobalt.[9, 56] It is important to note that in the present case, no co-catalysts are added and that the overall splitting activity arises from the intrinsic efficiency of MOFs. Of the two simultaneously occurring reactions, i.e. hydrogen evolution and water oxidation, the latter is kinetically the most demanding reaction.[69] For this reason, it is a common practice to determine the photocatalytic hydrogen evolution in the presence of sacrificial electron donors that typically increase the efficiency of hydrogen generation by more than one order of magnitude.[8] In the present case, in the irradiation under UV-visible using UiO-66(Zr/Ce/Ti) as photocatalyst addition of methanol as sacrificial electron donor increases the amount of hydrogen evolved by two-fold reaching a value after 22 h of 390 μmoles g^{-1} catalyst. This modest influence of the presence of methanol on the photocatalytic hydrogen generation indicates that hole quenching by water with the evolution of oxygen production is, in the present case, a process that occurs at relatively high reaction rate compared to other photocatalytic systems. Therefore, that does not cause the expected slowdown of the photocatalytic process. Since oxygen evolution by water oxidation is a four electrons-four protons process, it is proposed that the multimetallic

$M_6^{IV}O_4(OH)_4^{12-}$ clusters of UiO-66 are acting somehow similarly to the multimetallic oxygen evolution center in the natural photosynthetic center II, cooperatively removing the electrons and protons required in the transformation of H_2O into O_2. In other words, the presence of three metals with different oxidation potentials in the same M^{IV}_6 cluster could store in close spatial proximity more than one hole, while providing coordination sites for water, hydroxyl andother oxygen intermediates, making easier the formation of O_2.

3.2 **Mechanism of the photocatalytic water splitting**

In order to get more insights on the most photoactive material prepared in this work UiO-66(Zr/Ti/Ce) the band energy was experimentally determined. In particular, a valence band energy vs. vacuum of -7.05 eV was estimated from XPS and the band gap of 3.10 eV was measured by diffuse reflectance UV-Vis spectroscopy, resulting in a conduction band energy minimum vs. vacuum of -3.95 eV. These data confirm that the UiO-66(Zr/Ti/Ce) band alignment is appropriate to promote overall water splitting at pH 7 that requires CB of higher than -4.03 eV and VB lower than -5.26 eV for H_2 and O_2 evolution from water, respectively (**Figure S29**).

To assess the occurrence of charge separation upon irradiation of mixed metal UiO-66(Zr/Ce/Ti), irradiation of acetonitrile suspensions of this material in the presence of N,N,N',N'-tetramethyl-p-phenylenediamine (TMPDA) and methyl viologen (MV^{2+}), two typical visual probes of photooxidation and photoreduction,[70, 71] respectively, was carried out. As indicated in **Scheme 1**, upon excitation of the linker in UiO-66(Zr/Ce/Ti) ligand-to-metal charge transfer should occur with the simultaneous generation of electrons in the LUCO and positive holes at the HOCO; these electrons and holes can be quenched by suitable electron acceptors (MV^{2+}) or electron donors (TMPDA).

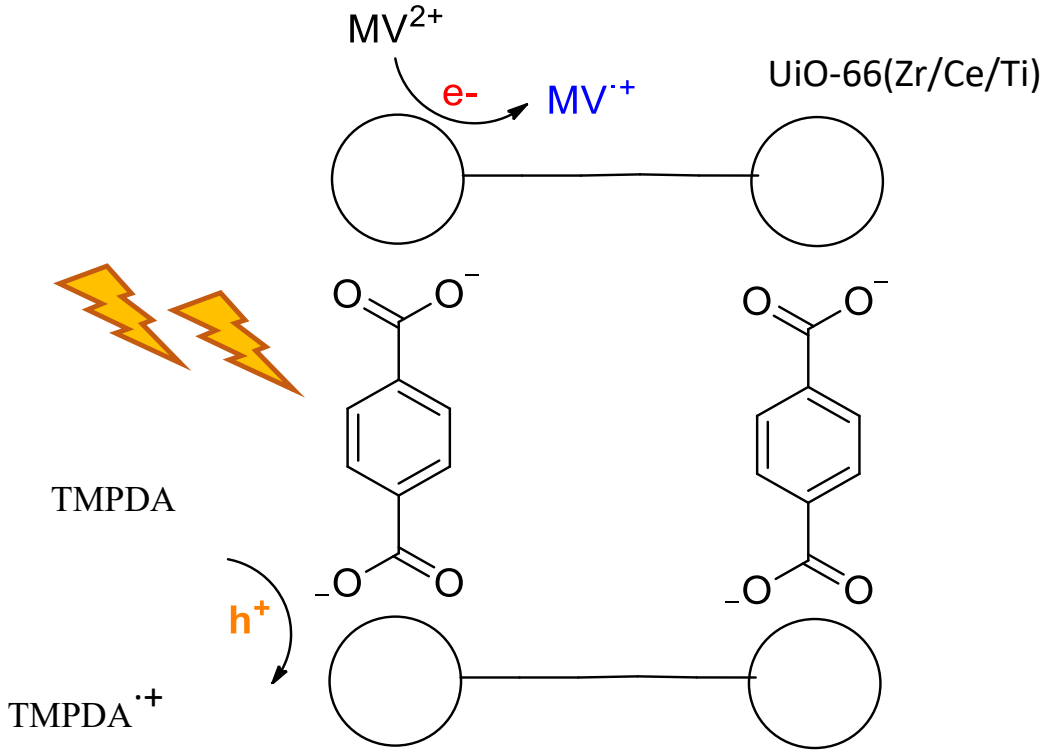

Scheme 1. Proposed photoinduced electron transfer process upon light excitation and generation of radical cation by MV^{2+} reduction and TMPDA oxidation.

The use of these quenchers in particular results in the generation of the corresponding radical cations that can be visually observed by their characteristic color and their generation can be conveniently followed by colorimetric techniques. These data could be also used to quantify the concentration of these radical cations. **Figure 4** shows the absorption spectrum of an acetonitrile suspension of UiO-66(Zr/Ce/Ti) containing TMPDA before and after irradiation. Upon irradiation the characteristic absorption band corresponding to $TMPDA^{\cdot+}$ radical cation, that exhibits an absorption band with fine structure centered at 590 nm, can be seen.[70, 71] The inset in **Figure 4** shows a photograph of the suspension upon irradiation showing the characteristic color of the photo-generated $TMPDA^{\cdot+}$.

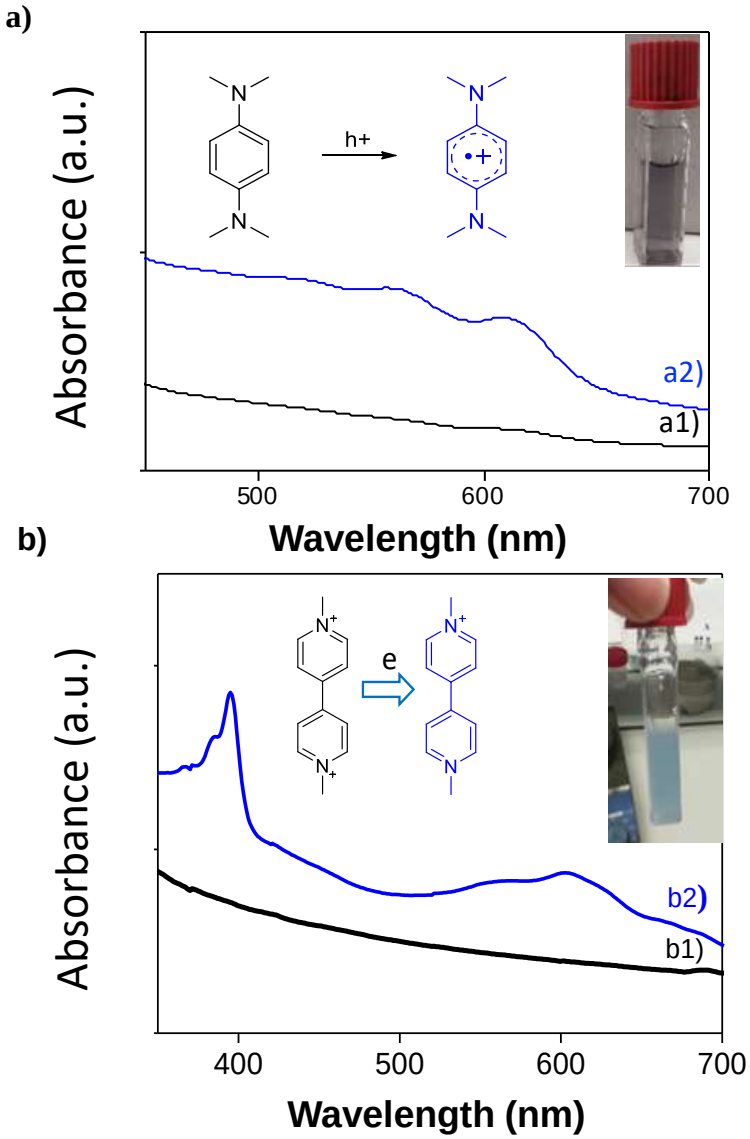

Figure 4. UV−vis absorption spectra of an acetonitrile suspension of the UiO-66(Zr/Ce/Ti) MOF in the presence of: TMPDA as electron donor a), before a1) and after a2) solar simulator irradiation, and MV^{2+}, as electron acceptor b), before (b1) and after (b2) xenon lamp irradiation. The photographs of the insets show the visual appearance of the suspensions under each condition.

While the use of TMPDA as probe shows the occurrence of oxidation upon simulated sunlight irradiation of UiO-66(Zr/Ce/Ti) as photocatalyst, an analogous experiment was carried out with MV^{2+}, as electron acceptor. In this case the suspension becomes blue and optical spectroscopy shows the characteristic UV-Vis spectrum of $MV^{\cdot+}$ radical cation that exhibits a sharp peak at 390 nm with a shoulder in the blue side and a much less intense broad peak with fine structure at 600 nm.

Formation of $MV^{\cdot+}$ radical cation indicates the photogeneration of electrons upon irradiation of UiO-66(Zr/Ce/Ti).

After having shown the occurrence of charge separation upon irradiation of UiO-66(Zr/Ce/Ti) with generation of electrons and holes, it is of interest to determine the possible origin of the higher photocatalytic activity of trimetallic UiO-66(Zr/Ce/Ti) in comparison with monometallic and bimetallic analogues. Towards this goal, emission spectra of the samples suspended in acetonitrile were recorded. The results are presented in **Figure 5**. As it can be seen there, two samples, namely UiO-66(Zr) and UiO-66(Zr/Ti) exhibit emission in the range from 350-600 nm.

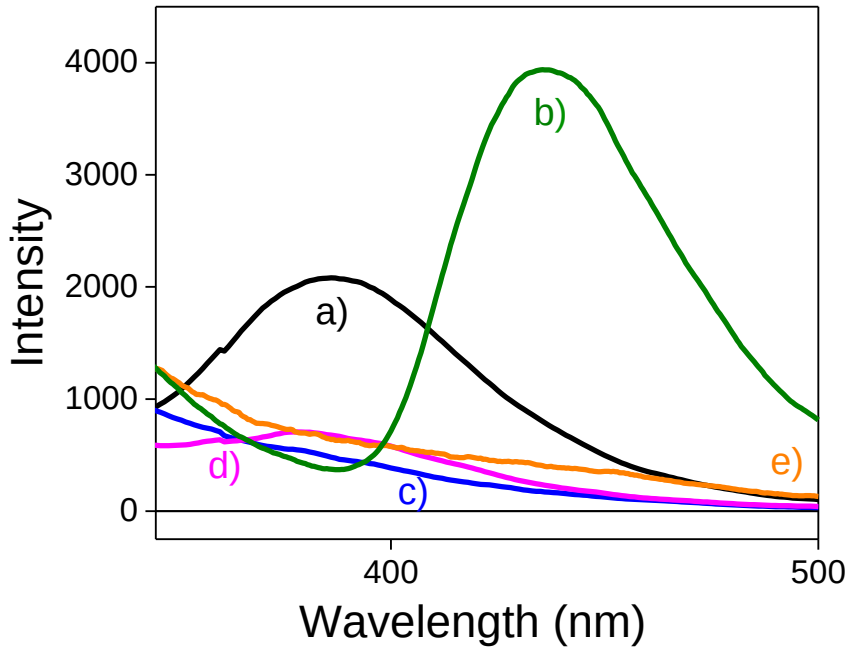

Figure 5. Emission spectra (λ_{exc}= 266 nm) of acetonitrile suspensions of a) UiO-66(Zr), b) UiO-66(Zr/Ti), c) UiO-66(Zr/Ce), d) UiO-66(Zr/Ce/Ti), and e) UiO-66(Ce).

The emission intensity follows the order UiO-66(Zr/Ti)>UiO-66(Zr). Since the most removable origin of this emission is the energy dissipation of electron-hole recombination, the higher the emission intensity, the higher the electron-hole recombination. Therefore, the fact that trimetallic UiO-66(Zr/Ce/Ti) does not emit indicates that, for this material, charge recombination occurs in

much lesser extent than for the other samples. Charge recombination is an undesirable energy waste process, competing with photocatalyst.

This relative emission intensity is, therefore, compatible with the higher photocatalytic efficiency of UiO-66(Zr/Ce/Ti) that should become favored as the percentage of charge recombination, related to the emission intensity decreases.

Transient absorption spectroscopy measurements were carried out to further understand the origin of the enhanced photocatalytic activity. In one of the series of the experiments, aqueous solution of the terephthalate ligand was irradiated with a nanosecond 266 nm laser pulse. A transient decay in the microsecond time scale, attributed to the photogeneration of the terephthalic triplet exited state, was recorded. The influence of the presence of the metals present in the nodes of UiO-66 to this transient excited state was studied by monitoring the transient signals at 330 nm. It was observed that the transient signal corresponding to the terephthalic triplet exited state is quenched by $Zr_6O_4(OH)_4^{-12}$, that was prepared previously to be used in the quenching experiment. **Figure 6** shows the change in the terephthalate transient signal in the absence and in the presence of the $[Zr_6O_4(OH)_4]^{-12}$ cluster.

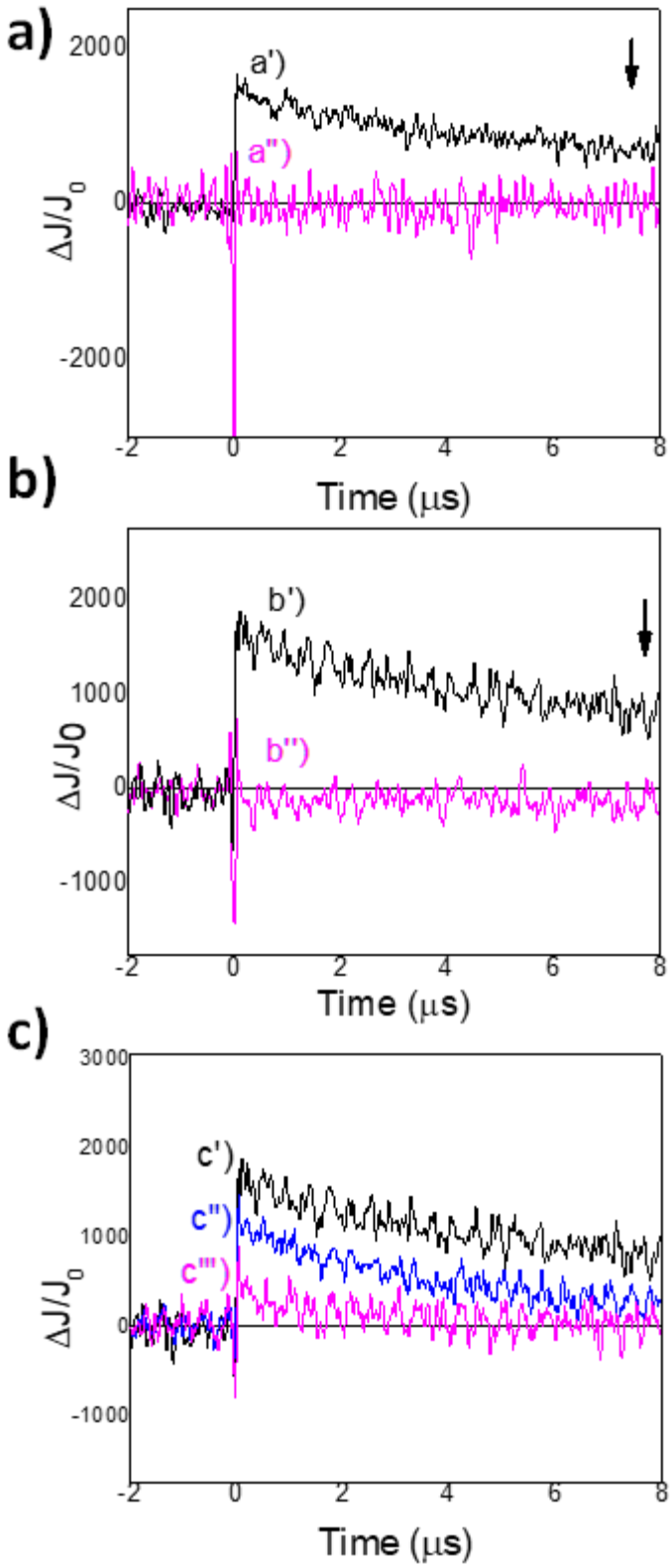

Figure 6. a) Temporal profiles of the transient signal monitored at 330 nm for an aqueous solution of the terephthalate ligand at pH 12: before a') and after a'') the addition of an aqueous solution of $Zr_6O_4(OH)_4$ ($7.5x10^{-4}$ M); before b') and after b'') the addition of an aqueous solution of $TiCl_4$ ($1.0x10^{-4}$ M) and before c') and after the addition of an aqueous solution of Ce $(NH_4)_2(NO_3)_6$ ($0.5x10^{-4}$ M, c'') and $10.0x10^{-4}$M c''')).

Similarly, terephthalate transient signal was quenched by the presence of $TiCl_4$ and $Ce(NH_4)_2(NO_3)_6$, although for these two cases the quenching rate constant was significantly lower than for the case of $Zr_6O_4(OH)_4^{12-}$ cluster (quenching rate constant values are k: $[Zr_6O_4(OH)_4]^{12-}$ = 71216 M^{-1}; k $TiCl_4$ = 45839 M^{-1}; k Ce $(NH_4)_2(NO_3)_6$= 48187 M^{-1}) . Although the Ti^{4+} and Ce^{4+} species may not exactly correspond to the UiO-66 metal clusters, this quenching study in solution proves that the triplet excited state of the terephthalate linker can interact with the clusters or cations present in the UiO-66(Zr/Ce/Ti) node.

Additional measurements were carried out with all the solid UiO-66 samples in acetonitrile suspensions. It has been reported in literature that photogenerated transients can be conveniently monitored using persistent suspensions of these semiconductors.[8] To address the nature of the transient signals, dichloromethane as electron quencher and methanol as hole quencher were employed. Upon excitation of acetonitrile suspensions of the five UiO-66 samples, transient signals spanning the whole range of UV and visible wavelengths were observed. The intensity of the absorbance increases toward the red region of the spectrum in three of the samples containing Zr and in UiO-66(Ce), while UiO-66(Zr/Ti) presents a neutral absorbance intensity through the whole range of wavelength (**Figure 7**).

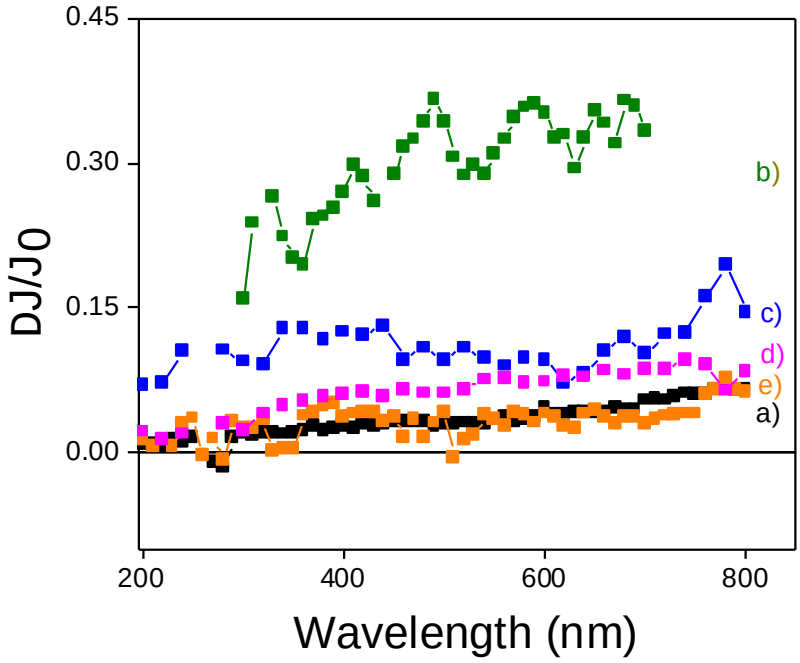

Figure 7. Transmission transient absorption spectra of a) UiO-66(Zr), b) UiO-66(Zr/Ti), c) UiO-66(Zr/Ce), d) UiO-66(Zr/Ce/Ti) and e) UiO-66(Ce) MOF recorded 1.4 μs after 266 nm laser excitation under argon atmosphere for optically matched (absorbance 0.1) suspensions of the UiO-66 solids in acetonitrile.

Two different behaviors in the presence of quenchers were observed. In the case of monometallic UiO-66(Zr), UiO-66(Ce) as well as trimetallic UiO-66(Zr/Ce/Ti) the transient signal is quenched both by addition of dichloromethane and methanol. This quenching behavior indicates that transient signals in the whole spectral range correspond to the combined absorption of electrons and holes. In agreement with the quenching, the signal monitored at 400 nm becomes faster in the presence of both quenchers. To illustrate this behavior **Figure 8** shows the case of the most efficient trimetallic UiO-66(Zr/Ce/Ti) photocatalyst.

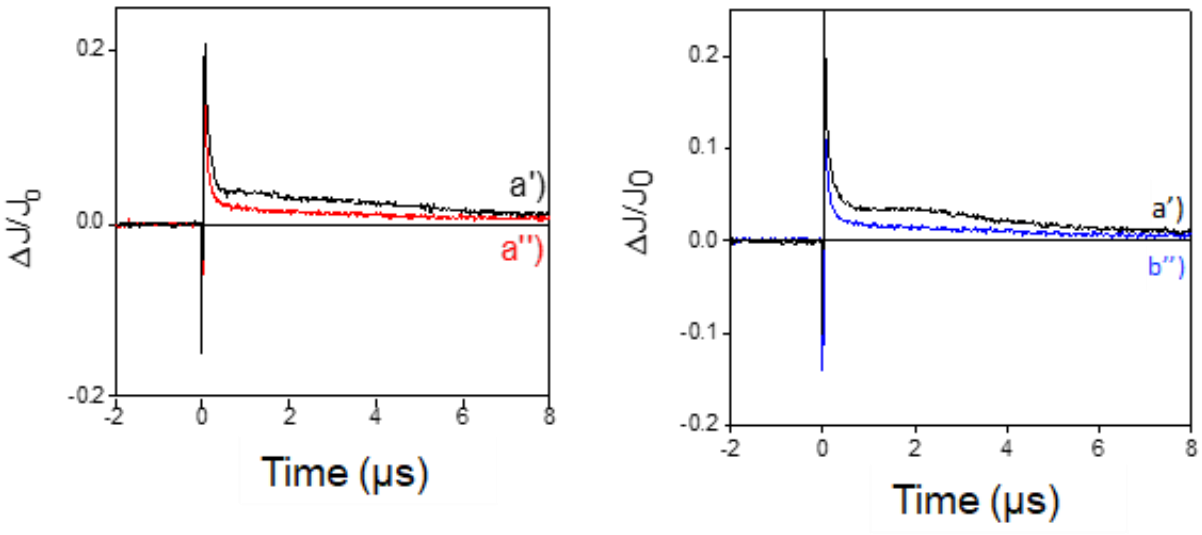

Figure 8. Temporal profile of the transient signals monitored at 400 nm for UiO-66(Zr/Ce/Ti) recorded upon 266 nm laser excitation under argon atmosphere a'), and after addition of 300 μL of dichloromethane a'') and methanol b'').

The two bimetallic MOFs, UiO-66(Zr/Ti) and UiO-66(Zr/Ce) exhibit a contrasting behavior. The transient signals are quenched by the presence of methanol, but in the presence of dichloromethane, the intensity of the transient signals and the lifetime of the transient species increase for UiO-66(Zr/Ti), while for UiO-66(Zr/Ce) a moderate quenching in the intensity, but not in the lifetime can be seen. This indicates that for UiO-66(Zr/Ti) the main component contributing to the monitored transient signals are photogenerated holes that disappear in the presence of methanol but increase in intensity in the presence of dichloromethane due to the lesser extent of electron-hole recombination, when an electron scavenger is present. Supporting information presents a more complete set of transient spectra in the presence of these two quenchers (**Figures S30-S33**). Overall, the time resolved study agrees with the generation of a charge separated state decaying in a few μs with two kinetics (**Figure 9**): one fast that is complete in less than one microsecond corresponding to about 65% of the total initial signal and another slower spanning a few microseconds.

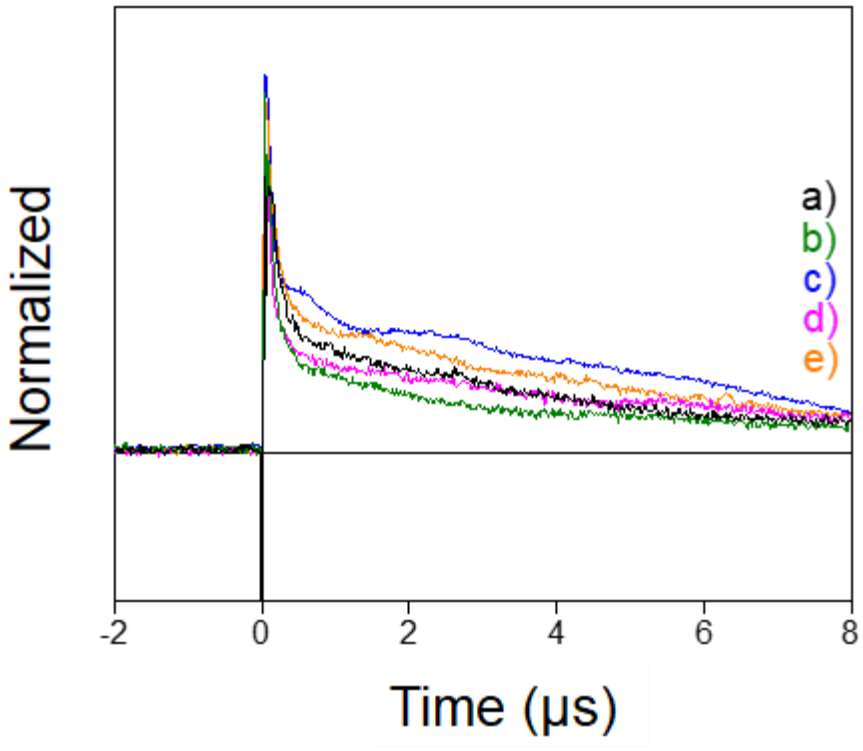

Figure 9. Temporal profile of the transient signals monitored at 400 nm recorded upon 266 nm laser excitation under argon atmosphere for a) UiO-66(Zr), b) UiO-66(Zr/Ti), c) UiO66-(Zr/Ce), d) UiO-66(Zr/Ce/Ti), e) UiO-66(Ce) MOFs.

This temporal profile indicates the occurrence of a fast charge recombination of 50 to 70 % of the photogenerated electrons and holes in less than one microsecond and relocation of the remaining percentage of charge carriers resulting in a longer-lived charge separation state that finally disappears at a longer timescale. The presence of quenchers alters both the fast and the slower regime, indicating that both types of charge carriers are accessible to the quenchers. A summary of the kinetic data obtained from the time resolved measurements are summarized in **Table S1** of the supporting information.

Importantly, the dynamic behavior of the trimetallic UiO-66(Zr/Ce/Ti) does not differ significantly from that of monometallic UiO-66(Zr), since the transient signals and the percentage of the slowest components are similar. Therefore, it is suggested that the higher efficiency observed in overall water splitting should be related to the efficiency of charge separation and the lesser degree of

change recombination resulting in a higher density of electrons and holes for the trimetallic UiO-66(Zr/Ce/Ti), rather than in the kinetics, lifetime and decay of the charge separated state.

3. **Conclusions**

A computational study has suggested that UiO-66(Ce) should be a suitable photocatalyst for overall water splitting. However, the present study has provided experimental that, instead of monometallic MOFs, mixed metal UiO-66 are more efficient, particularly trimetallic UiO-66(Zr/Ce/Ti). For this material a high percentage of the photocatalytic activity, over 40%, derives from visible light photo-response. Photocatalytic experiments using methanol as sacrificial electron donor indicate that oxygen generation is considerably favored in trimetallic UiO-66, a fact that has been attributed to the collective cooperation of trimetallic clusters favoring the kinetics of the four electrons-four proton process resulting in oxygen evolution. Time resolved measurements in acetonitrile suspensions have allowed to detect the charge separation state in the microsecond time scale. The transient signals correspond to a combination of electrons and holes in the complete UV-Vis wavelength range, both for UiO-66(Zr) and UiO-66(Zr/Ce/Ti), with similar kinetic behavior. In contrast with the similar charge separation state kinetics, photoluminescence measurements reveal much lesser emission intensity for trimetallic UiO-66(Zr/Ce/Ti) than for monometallic UiO-66(Zr), indicating that unfavorable charge recombination occurs for UiO-66(Zr/Ce/Ti) in much lesser extent than in the other UiO-66 congeners. Thus, the multimetallic composition favors higher generation of charge separation, increasing the photocatalytic efficiency of this material. Overall, the present study shows the opportunity that MOFs offer to prepare efficient visible-light photocatalysts for overall water splitting, something that has been challenging for metal oxide semiconductors.

Acknowledgements
Financial support by the Spanish Ministry of Science and Innovation (Severo Ochoa and RTI2018-098237-CO21) and Generalitat Valenciana (Prometeo 2017/083) is gratefully acknowledged. S.N. thanks financial support by the Fundación Ramón Areces (XVIII Concurso Nacional para la Adjudicación de Ayudas a la Investigación en Ciencias de la Vida y de la Materia, 2016), Ministerio de Ciencia, Innovación y Universidades RTI2018-099482-A-I00 project and Generalitat Valenciana grupos de investigación consolidables 2019 (ref: AICO/2019/214) project.

References

[1] H. Li, M. Eddaoudi, M. O'Keeffe, O.M. Yaghi, Design and synthesis of an exceptionally stable and highly porous metal- organic framework, Nature, 402 (1999) 276-279.
[2] G. Férey, C. Mellot-Draznieks, C. Serre, F. Millange, J. Dutour, S. Surblé, I. Margiolaki, A chromium terephthalate-based solid with unusually large pore volumes and surface area, Science, 23 (2005) 2040-2042.
[3] H. Furukawa, Cordova, K.E., O'Keeffe, M., Yaghi, O.M., The chemistry and applications of metal-organic frameworks, Science, 341 (2013) 1230444.
[4] T. Devic, C. Serre, High valence 3p and transition metal based MOFs, Chem.Soc.Rev.,, 43 (2014) 6097-6115.
[5] S. Kitagawa, R. Kitaura, S.-I. Noro, Functional porous coordination polymers, Angew. Chem. Int. Ed., 43 (2004) 2334-2375.
[6] O.M. Yaghi, M. O'Keeffe, N.W. Ockwig, H.K. Chae, M. Eddaoudi, J. Kim, Reticular synthesis and the design of new materials, Nature, 423 (2003) 705-714.
[7] H.-C. Zhou, J.R. Long, O.M. Yaghi, Introduction to metal-organic frameworks, Chem. Rev., 112 (2012) 673-674.
[8] A. Dhakshinamoorthy, A.M. Asiri, H. García, Metal-Organic Framework (MOF) Compounds: Photocatalysts for Redox Reactions and Solar Fuel Production, Angew. Chem. Int. Ed., 55 (2016) 5414-5445.
[9] X. Li, J. Yu, M. Jaroniec, X. Chen, Cocatalysts for Selective Photoreduction of CO2 into Solar Fuels, Chem. Rev., 119 (2019) 3962−4179.
[10] M. Cabrero-Antonino, S. Remiro-Buenamanaña, M. Souto, A.A. Garciá-Valdivia, D. Choquesillo-Lazarte, S. Navalón, A. Rodríguez-Diéguez, G. Mínguez Espallargas, H. Garciá, Design of cost-efficient and photocatalytically active Zn-based MOFs decorated with Cu O nanoparticles for CO2 methanation Chem. Commun., 55 (2019) 10932-10935
[11] D. Mateo, A. Santiago-Portillo, J. Albero, S. Navalón, M. Alvaro, H. García, Long-Term Photostability in Terephthalate Metal–Organic Frameworks, Angew. Chem. Int. Ed. (DOI: 10.1002/anie.201911600), (2019).
[12] H. García, S. Navalón, Metal-Organic Frameworks:Applications in Separations and Catalysis, Wiley, ISBN: 978-3-527-80910-3, 2018.
[13] I.I. Alkhatib, C. Garlisi, M. Pagliaro, K. Al-Ali, G. Palmisano, Metal-organic frameworks for photocatalytic CO2 reduction under visible radiation: A review of strategies and applications Catal. Today, 340 (2020) 209-224

[14] R. Li, W. Zhang, K. Zhou, Metal–Organic-Framework-Based Catalysts for Photoreduction of CO2, Adv. Mater., 30 (2018) 1705512.
[15] H. Luo, Z. Zeng, G. Zeng, C. Zhang, R. Xiao, D. Huang, C. Lai, M. Cheng, W. Wang, W. Xiong, Y. Yang, L. Qin, C. Zhou, H. Wang, Y. Zhou, S. Tian, Recent progress on metal-organic frameworks based- and derived-photocatalysts for water splitting, Chem. Eng. J., (2019) 123196.
[16] Y. Shi, A.-F. Yang, C.-S. Cao, B. Zhao, Applications of MOFs: Recent advances in photocatalytic hydrogen production from water, Coord. Chem. Rev., 390 (2019) 50-75
[17] C.G. Silva, I. Luz, F.X. Llabrés I Xamena, A. Corma, H. García, Water stable Zr-Benzenedicarboxylate metal-organic frameworks as photocatalysts for hydrogen generation, Chem. Eur. J., (2010) 11133-11138.
[18] S. Wang, X. Wang, Multifunctional Metal–Organic Frameworks for Photocatalysis Small, 26 (2015) 3097-3112.
[19] H.-Q. Xu, J. Hu, D. Wang, Z. Li, Q. Zhang, Y. Luo, S.-H. Yu, H.-L. Jiang, Visible-Light Photoreduction of CO2 in a Metal–Organic Framework: Boosting Electron–Hole Separation via Electron Trap States, J. Am. Chem. Soc., 137 (2015) 13440-13443.
[20] S.-N. Zhao, G. Wang, D. Poelman, P. Van Der Voort, Metal Organic Frameworks Based Materials for Heterogeneous Photocatalysis, Molecules, 23 (2018) 2947.
[21] A. Jamal Sisi, M. Fathinia, A. Khataee, Y. Orooji, Systematic activation of potassium peroxydisulfate with ZIF-8 via sono-assisted catalytic process: Mechanism and ecotoxicological analysis, Journal of Molecular Liquids, 308 (2020) 113018.
[22] M.A. Nasalevich, C.H. Hendon, J.G. Santaclara, K. Svane, B. van der Linden, S.L. Veber, M. Fedin, A.J. Houtepen, M.A. van der Veen, F. Kapteijn, A. Walsh, J. Gascon, Electronic origins of photocatalytic activity in d0 metal organic frameworks, Sci. Rep., 6 (2016) 23676.
[23] M.A. Nasalevich, M. Van Der Veen, F. Kapteijn, J. Gascon, Metal-organic frameworks as heterogeneous photocatalysts: Advantages and challenges, CrystEngComm, 16 (2014) 4919-4926.
[24] J.G. Santaclara, F. Kapteijn, J. Gascon, M.A. Van Der Veen, Understanding metal-organic frameworks for photocatalytic solar fuel production, CrystEngComm, 19 (2017) 4118-4125
[25] A. Santiago-Portillo, H.G. Baldoví, M.T.G. Fernandez, S. Navalón, P. Atienzar, B. Ferrer, M. Alvaro, H. Garcia, Z. Li, Ti as Mediator in the Photoinduced Electron Transfer of Mixed-Metal NH2–UiO-66(Zr/Ti): Transient Absorption Spectroscopy Study and Application in Photovoltaic Cell, J. Phys. Chem. C, 121 (2017) 7015-7024.
[26] L. Wang, P. Jin, S. Duan, H. She, J. Huang, Q. Wang, In-situ incorporation of Copper(II) porphyrin functionalized zirconium MOF and TiO2 for efficient photocatalytic CO2 reduction, Science Bulletin, 64 (2019) 926-933.
[27] J. Qiu, X. Zhang, Y. Feng, X. Zhang, H. Wang, J. Yao, Modified metal-organic frameworks as photocatalysts, Appl. Catal. B. Environ., 231 (2018) 317-342
[28] F. Khodadadian, M. Nasalevich, F. Kapteijn, A.I. Stankiewicz, R. Lakerveld, J. Gascon, Photocatalysis: Past Achievements and Future Trends, Alternative Energy Sources for Green Chemistry2016, pp. 227-269.
[29] M. Shekofteh-Gohari, A. Habibi-Yangjeh, M. Abitorabi, A. Rouhi, Magnetically separable nanocomposites based on ZnO and their applications in photocatalytic processes: A review, Critical Reviews in Environmental Science and Technology, 48 (2018) 806-857.
[30] M. Salavati-Niasari, Synthesis and Characterization of Host (Nanodimensional Pores of Zeolite-Y)–Guest [Unsaturated 16-Membered Octaaza–macrocycle Manganese(II), Cobalt(II), Nickel(II), Copper(II), and Zinc(II) Complexes] Nanocomposite Materials, Chemistry Letters, 34 (2005) 1444-1445.
[31] M. Pirhashemi, A. Habibi-Yangjeh, S. Rahim Pouran, Review on the criteria anticipated for the fabrication of highly efficient ZnO-based visible-light-driven photocatalysts, Journal of Industrial and Engineering Chemistry, 62 (2018) 1-25.
[32] M. Ghanbari, M. Salavati-Niasari, Tl4CdI6 Nanostructures: Facile Sonochemical Synthesis and Photocatalytic Activity for Removal of Organic Dyes, Inorganic Chemistry, 57 (2018) 11443-11455.

[33] P. Mehdizadeh, Y. Orooji, O. Amiri, M. Salavati-Niasari, H. Moayedi, Green synthesis using cherry and orange juice and characterization of TbFeO3 ceramic nanostructures and their application as photocatalysts under UV light for removal of organic dyes in water, Journal of Cleaner Production, 252 (2020) 119765.
[34] Y. Orooji, R. Mohassel, O. Amiri, A. Sobhani, M. Salavati-Niasari, Gd2ZnMnO6/ZnO nanocomposites: Green sol-gel auto-combustion synthesis, characterization and photocatalytic degradation of different dye pollutants in water, Journal of Alloys and Compounds, 835 (2020) 155240.
[35] Y. Orooji, A.a. Alizadeh, E. Ghasali, M.R. Derakhshandeh, M. Alizadeh, M.S. Asl, T. Ebadzadeh, Co-reinforcing of mullite-TiN-CNT composites with ZrB2 and TiB2 compounds, Ceramics International, 45 (2019) 20844-20854.
[36] F. Mohandes, F. Davar, M. Salavati-Niasari, Magnesium oxide nanocrystals via thermal decomposition of magnesium oxalate, Journal of Physics and Chemistry of Solids, 71 (2010) 1623-1628.
[37] M. Salavati-Niasari, M.R. Loghman-Estarki, F. Davar, Controllable synthesis of nanocrystalline CdS with different morphologies by hydrothermal process in the presence of thioglycolic acid, Chemical Engineering Journal, 145 (2008) 346-350.
[38] M. Salavati-Niasari, Ship-in-a-bottle synthesis, characterization and catalytic oxidation of styrene by host (nanopores of zeolite-Y)/guest ([bis(2-hydroxyanil)acetylacetonato manganese(III)]) nanocomposite materials (HGNM), Microporous and Mesoporous Materials, 95 (2006) 248-256.
[39] M. Sabet, M. Salavati-Niasari, O. Amiri, Using different chemical methods for deposition of CdS on TiO2 surface and investigation of their influences on the dye-sensitized solar cell performance, Electrochimica Acta, 117 (2014) 504-520.
[40] L. Wang, S. Duan, P. Jin, H. She, J. Huang, Z. Lei, T. Zhang, Q. Wang, Anchored Cu(II) tetra(4-carboxylphenyl)porphyrin to P25 (TiO2) for efficient photocatalytic ability in CO2 reduction, Applied Catalysis B: Environmental, 239 (2018) 599-608.
[41] M.A. Syzgantseva, C.P. Ireland, F.M. Ebrahim, B. Smit, O.A. Syzgantseva, Metal Substitution as the Method of Modifying Electronic Structure of Metal−Organic Frameworks, J. Am. Chem. Soc., 141 (2019) 6271−6278.
[42] X.-P. Wu, L. Gagliardi, D.G. Truhlar, Cerium Metal−Organic Framework for Photocatalysis, J. Am. Chem. Soc., 140 (2018) 7904-7912.
[43] X.-P. Wu, L. Gagliardi, D.G. Truhlar, Metal doping in cerium metal-organic frameworks for visible-response water splitting photocatalysts, J. Chem. Phys., 150 (2019) 041701.
[44] D. Sun, W. Liu, M. Qiu, Y. Zhang, Li, Z. , Introduction of a mediator for enhancing photocatalytic performance via post-synthetic metal exchange in metal-organic frameworks (MOFs), Chem. Commun., 51 (2015) 2056-2059.
[45] M. Salavati-Niasari, Nanoscale microreactor-encapsulation of 18-membered decaaza macrocycle nickel(II) complexes, Inorganic Chemistry Communications, 8 (2005) 174-177.
[46] M.A. Nasalevich, M.G. Goesten, T.J. Savenije, F. Kapteijn, J. Gascon, Enhancing optical absorption of metal–organic frameworks for improved visible light photocatalysis, Chemical Communications, 49 (2013) 10575-10577.
[47] M. Salavati-Niasari, A. Sobhani, F. Davar, Synthesis of star-shaped PbS nanocrystals using single-source precursor, Journal of Alloys and Compounds, 507 (2010) 77-83.
[48] J.H. Cavka, S. Jakobsen, U. Olsbye, N. Guillou, C. Lamberti, S. Bordiga, K. Lillerud, A new zirconium inorganic building brick forming metal organic frameworks with exceptional stability. , J. Am. Chem. Soc., 130 (2008) 13850-13851.
[49] L. Valenzano, B. Civalleri, S. Chavan, S. Bordiga, M.H. Nilsen, S. Jakobsen, K.P. Lillerud, C. Lamberti, Disclosing the Complex Structure of UiO-66 Metal Organic Framework: A Synergic Combination of Experiment and Theory, Chem. Mater., 23 (2011) 1700-1718.

[50] Y. Lee, S. Kim, J.K. Kang, C. S.M., Photocatalytic CO2 reduction by a mixed metal (Zr/Ti), mixed ligand metal–organic framework under visible light irradiation, Chem. Commun., 51 (2015) 5735-5738.
[51] F. Nouar, M.I. Breeze, B.C. Campo, A. Vimont, G. Clet, M. Daturi, T. Devic, R.I. Walton, C. Serre, Tuning the properties of the UiO-66 metal organic framework by Ce substitution, Chem. Commun., 51 (2015) 14458-14461.
[52] K. Hendrickx, J.J. Joos, A. De Vos, D. Poelman, P.F. Smet, V. Van Speybroeck, P. Van Der Voort, K. Lejaeghere, Exploring lanthanide doping in UiO-66: a combined experimental and computational study of the electronic structure, Inorganic chemistry, 57 (2018) 5463-5474.
[53] A. Akhundi, A. Badiei, G.M. Ziarani, A. Habibi-Yangjeh, M.J. Muñoz-Batista, R. Luque, Graphitic carbon nitride-based photocatalysts: Toward efficient organic transformation for value-added chemicals production, Molecular Catalysis, 488 (2020) 110902.
[54] P. Frontera, A. Macario, M. Ferraro, P. Antonucci, Supported catalysts for CO2 methanation: a review, Catalysts, 7 (2017) 59.
[55] Y. An, B. Xu, Y. Liu, Z. Wang, P. Wang, Y. Dai, X. Qin, X. Zhang, B. Huang, Photocatalytic Overall Water Splitting over MIL-125(Ti) upon CoPi and Pt Co-catalyst Deposition, ChemistryOpen, 6 (2017) 701 – 705.
[56] S. Remiro-Buenamañana, M. Cabrero-Antonino, M. Martínez-Guanter, M. Álvaro, S. Navalón, H. García, Influence of co-catalysts on the photocatalytic activity of MIL-125(Ti)-NH2 in the overall water splitting Appl. Catal. B. Environ., (2019) 677-684.
[57] S. Gholamrezaei, M. Salavati-Niasari, Sonochemical synthesis of SrMnO3 nanoparticles as an efficient and new catalyst for O2 evolution from water splitting reaction, Ultrasonics Sonochemistry, 40 (2018) 651-663.
[58] M. Ghasemi, A. Khataee, P. Gholami, R.D.C. Soltani, A. Hassani, Y. Orooji, In-situ electro-generation and activation of hydrogen peroxide using a CuFeNLDH-CNTs modified graphite cathode for degradation of cefazolin, Journal of Environmental Management, 267 (2020) 110629.
[59] M. Lammert, C. Glißmann, N. Stock, Tuning the stability of bimetallic Ce(IV)/Zr(IV)-based MOFs with UiO-66 and MOF-808 structures, Dalton Trans., 46 (2017) 2425-2429.
[60] A. Santiago-Portillo, S. Navalón, M. lvaro, H. García, Generating and optimizing the catalytic activity in UiO-66 for aerobic oxidation of alkenes by post-synthetic exchange Ti atoms combined with ligand substitution, J. Catal., 365 (2018) 450-463.
[61] K.A. Lomachenko, J. Jacobsen, A.L. Bugaev, C. Atzori, F. Bonino, S. Bordiga, N. Stock, C. Lamberti, Exact stoichiometry of CexZr6-x cornerstones in mixedmetal UiO-66 MOFs revealed by EXAFS spectroscopy, J. Am. Chem. Soc., 140 (2018) 17379-17383.
[62] Y. Zhang, H. Chen, Y. Pan, X. Zeng, X. Jiang, Z. Long, X. Hou, Cerium-based UiO-66 metal–organic frameworks explored as efficient redox catalysts: titanium incorporation and generation of abundant oxygen vacancies, Chemical Communications, 55 (2019) 13959-13962.
[63] M. Kim, J.F. Cahill, H. Fei, K.A. Prather, S.M. Cohen, Postsynthetic ligand and cation exchange in robust metal–organic frameworks, Journal of the American Chemical Society, 134 (2012) 18082-18088.
[64] A. De Vos, K. Hendrickx, P. Van Der Voort, V. Van Speybroeck, K. Lejaeghere, Missing linkers: an alternative pathway to UiO-66 electronic structure engineering, Chemistry of Materials, 29 (2017) 3006-3019.
[65] A. Buragohaina, S. Biswas, Cerium-based azide- and nitro-functionalized UiO-66 frameworks as turn-on fluorescent probes for the sensing of hydrogen sulphide, CrystEngComm 18 (2016) 4374-4381.
[66] M. Lammert, M.T. Wharmby, S. Smolders, B. Bueken, A. Lieb, K.A. Lomachenko, D. De Vos, N. Stork, Cerium-Based metal organic frameworks with UiO-66 architeture: synthesis, properties and redox catalytic activity, Chem. Comm., 51 (2015) 12578-12581.

[67] Q. Liu, H. Cong, H. Deng, Deciphering the spatial arrangement of metals and correlation to reactivity in multivariate metal–organic frameworks, Journal of the American Chemical Society, 138 (2016) 13822-13825.
[68] F. Trousselet, A. Archereau, A. Boutin, F.-X. Coudert, Heterometallic Metal–Organic Frameworks of MOF-5 and UiO-66 Families: Insight from Computational Chemistry, The Journal of Physical Chemistry C, 120 (2016) 24885-24894.
[69] Z. Wang, C. Li, K. Domen, Recent developments in heterogeneous photocatalysts for solar-driven overall water splitting, Chem. Soc. Rev., 48 (2019) 2109-2125
[70] M. Alvaro, E. Carbonell, B. Ferrer, F.X. Llabrés i Xamena, H. Garcia, Chem. Eur. J., 13 (2007) 5106-5112.
[71] M. De Miguel, F. Ragon, T. Devic, C. Serre, P. Horcajada, H. García, Evidence of photoinduced charge separation in the metal-organic framework MIL-125(Ti)-NH2 13 (2012) 3651-3654.

Graphical abstract